Understanding mixing of Ni and Pt in the Ni/Pt(111) bimetallic catalyst via molecular simulation and experiments

Hangyao Wang, Michail Stamatakis, Danielle A. Hansgen, Stavros Caratzoulas, and Dionisios G. Vlachos

Citation: The Journal of Chemical Physics **133**, 224503 (2010); doi: 10.1063/1.3512644
View online: http://dx.doi.org/10.1063/1.3512644
View Table of Contents: http://scitation.aip.org/content/aip/journal/jcp/133/22?ver=pdfcov
Published by the AIP Publishing

Understanding mixing of Ni and Pt in the Ni/Pt(111) bimetallic catalyst via molecular simulation and experiments

Hangyao Wang, Michail Stamatakis, Danielle A. Hansgen, Stavros Caratzoulas,[a] and Dionisios G.Vlachos[b]

Center for Catalytic Science and Technology, Catalysis Center for Energy Innovation, Department of Chemical Engineering, University of Delaware, Newark, Delaware 19716, USA

(Received 26 August 2010; accepted 18 October 2010; published online 9 December 2010)

Molecular dynamics (MD) simulations employing embedded atom method potentials and ultrahigh vacuum (UHV) experiments were carried out to study the mixing process between the Ni and Pt atoms in the Ni/Pt(111) bimetallic system. The barrier for a Ni atom to diffuse from the top surface to the subsurface layer is rather high (around 1.7 eV) as calculated using the nudged elastic band (NEB) method. Analysis of the relaxation dynamics of the Ni atoms showed that they undergo diffusive motion through a mechanism of correlated hops. At 600 K, all Ni atoms remain trapped on the top surface due to large diffusion barriers. At 900 K, the majority of Ni atoms diffuse to the second layer and at 1200 K diffusion to the bulk is observed. We also find that smaller Ni coverages and the presence of Pt steps facilitate the Ni–Pt mixing. By simulated annealing simulations, we found that in the mixed state, the Ni fraction oscillates between layers, with the second layer being Ni-richer at equilibrium. The simulation results at multiple time scales are consistent with the experimental data.
 [doi:10.1063/1.3512644]

I. INTRODUCTION

Bimetallic catalysts have gained considerable attention for many catalytic applications, such as hydrocarbon reforming and electrocatalysis, because they often exhibit improved reactivity and selectivity compared to their parent metals.[1–3] The unusual behavior of bimetallic catalysts has motivated extensive investigations on their potential applications as well as on the origins of enhanced reactivity (for a recent review, see Ref. 4). It is generally believed that the electronic and structural changes induced by the formation of bimetallic catalysts are responsible for the changes in reactivity and selectivity.[4,5] However, there has been a limited number of studies on the mechanism of bimetallic formation.

A Ni/Pt(111) bimetallic catalyst is typically prepared by depositing Ni atoms on a clean Pt(111) surface under ultrahigh vacuum (UHV) conditions.[6] Both submonolayer and one monolayer (ML) Ni/Pt(111) bimetallic catalysts have been studied experimentally. With the Ni layer in the subsurface, this system exhibits excellent activity and selectivity in hydrogenation reactions, attributed to weaker bonding of the hydrogen on the metal.[6–8] On the other hand, with the Ni layer on the top layer, this bimetallic catalyst is active in ammonia decomposition[9] and oxygenate reforming.[10] While the structure of bimetallic catalysts plays a crucial role in determining the reactivity, our understanding of the structure and mixing between two metals is limited. A notable study by Kitchin and co-workers[11] aimed at elucidating the surface morphology of the Ni/Pt(111) system using scanning tunneling microscopy (STM) and the origins of the weak metal–hydrogen bonding using temperature programmed desorption (TPD). Even though the STM images provided useful information on the growth of Ni films on the Pt(111) surface, they did not distinguish between Ni and Pt surface atoms. As a result, it is unclear what the surface structure looks like.

Density-functional theory (DFT) calculations have been carried out to study the stability of the Ni/Pt(111) bimetallic system.[12] However, most DFT studies of the full-monolayer Ni/Pt(111) system assume that the Ni layer is either the top one or the second one from the top (subsurface layer).[12] Because of cell size limitations in DFT calculations, it is difficult to capture the complex surface configurations of the material. Furthermore, DFT calculations cannot account for temperature effects as they are carried out at 0 K. These should be important in determining the surface structure of the Ni/Pt(111) catalyst, as STM and low-energy ion scattering spectroscopy (LEIS) studies have revealed that the Ni atoms remain on the Pt(111) surface at 300 K, but many of them diffuse into the bulk at 600 K.[11]

In order to understand the catalytic properties of the Ni/Pt(111) bimetallic catalyst, it is essential that we elucidate its surface structure and how it is affected, and ultimately determined, by factors such as temperature and Ni coverage, or by the topology of the Pt surface, like, for example, the presence of steps. These questions define the scope of the present computational study. Because of the multiple time scales present in the system, and thereby the possibility of trapping in long-lived metastable states, in this work we have used a number of computational tools. We have employed molecular dynamics (MD) to investigate the stability of an epitaxially deposited Ni layer on a Pt(111) substrate and to explore the relaxation dynamics. We have also performed simulated annealing simulations to ascertain whether the equilibrium state is characterized by complete mixing. In addition, we carried out nudged elastic band (NEB)

[a]Electronic mail: cstavros@udel.edu.
[b]Author to whom correspondence should be addressed. Electronic mail: vlachos@udel.edu.

calculations to explore the potential energy landscape, with emphasis on the diffusion of Ni out of the surface layer and on estimating the energy barriers associated with such diffusive motion. The computational findings are compared to UHV experiments conducted on the 1 ML Ni/Pt(111) system and to structure data available in the literature.

II. METHODS

A. Computational

The MD simulations were performed in the NVT ensemble using the large-scale atomic molecular massively parallel simulator (LAMMPS).[13] The force field was modeled with the embedded atom method (EAM),[14] which has been shown to be successful at describing the surface and bulk properties, such as surface relaxation and reconstruction, of metals and alloys.[15,16] The total potential energy of a system is given by

$$E_{\text{tot}} = \sum_{i}^{N} F_i(\rho_i) + \frac{1}{2} \sum_{i,j,i\neq j}^{N} \phi_{ij}(r_{ij}), \tag{1}$$

where i and j denote atoms. ρ_i denotes the background electron density at the position of atom i due to the electron densities of all other atoms, and is made up of additive, individual contributions which depend on the separation distance, r_{ij}, between atoms i and j:

$$\rho_i = \sum_{j,j\neq i} g_j(r_{ij}). \tag{2}$$

Here, $g_j(r_{ij})$ is the individual contribution of atom j to the electron density of atom i. In Eq. (1), $F_i(\rho_i)$ represents the embedding (attractive) energy of atom i into the background electron density ρ_i; and $\phi_{ij}(r_{ij})$ represents the core–core (repulsive) pair interaction between atoms i and j.

We modeled the Ni/Pt(111) system as a ten-layer slab containing nine layers of Pt and one layer of Ni (at different coverages). The bottom Pt layer was fixed at its bulk lattice geometry and periodic boundary conditions were enforced in the x-direction and y-direction. For the system with 1 ML Ni coverage, a starting configuration was constructed by placing the Ni atoms on top of the Pt(111) surface in a Pt-lattice geometry (lattice constant 3.92 Å). For the systems with a submonolayer Ni coverage, initial configurations were created by placing the Ni atoms at randomly selected fcc sites of the Pt(111) surface. The simulation cell dimensions were 2.77 nm × 2.88 nm, in the xy-plane, with each layer containing 120 atoms, for a total of 1200 atoms for the 1 ML Ni/Pt(111) system. The size of the simulation box was sufficient to eliminate periodic boundary conditions effects, as the interactions that make up the EAM force field are short-ranged. We have also tested a much larger cell size (8.32 nm × 8.64 nm), with each layer containing 1080 atoms, and indeed found that our results and conclusions were unaffected. The equations of motion were solved using the velocity Verlet algorithm,[17] and a time step of 1 femtosecond (fs) was sufficient to eliminate drifts in the total energy of the system. The system was coupled to a Nosé-Hoover thermostat with relaxation time 0.5 picosecond (ps).

The NEB (Ref. 18) calculations were run using the DL_Poly 2.19 simulation package.[19] In all these calculations the initial and final structures were optimized by running DL_Poly's programed optimization which involves both MD and conjugate gradients. The temperature was set to 1 K and the objective was to minimize energy with a tolerance of 0.0001 in DL_Poly units ($\approx 10^{-8}$ eV). The sequences of configurations used in the NEB calculations were constructed so that they closely follow pathways observed during the course of molecular dynamics simulations. The NEB results, combined with classical transition state theory (TST), can provide crude estimates of time scales to compare with both MD simulations and experimental data.

In order to explore the equilibrium structures, we have performed simulated annealing calculations according to the following protocol: heating up to 1800 K and then cooling down to 900 K at a rate of 1 K per 1000 steps (i.e., 10^{12} K/s). The results of these simulations may be thought of as being the very long time scale dynamics. All three techniques combined with the experiments provide information at various time scales.

B. Experimental

Experiments were performed to support the computational findings. In these experiments, Ni was deposited through physical vapor deposition onto a Pt(111) crystal. The surface is experimentally analogous to the Ni/Pt(111) surface studied in the MD simulations. In these experiments, a two-level stainless steel ultrahigh vacuum (UHV) chamber with an Auger electron spectrometer (AES) was used. The typical base pressure was below 5×10^{-10} Torr. The bimetallic surface was created by depositing Ni onto a Pt(111) crystal of 99.999% purity (Princeton Scientific Corp.). Before each experiment, the Pt(111) surface was cleaned with several Ne^+ sputter cycles, followed by 10 Langmuir (1 Langmuir (L) = 1×10^{-6} Torr s) oxygen to burn off any surface carbon. The crystal was then annealed at 1100 K for 5 min. This procedure was repeated until impurities were below the detection limit of AES. Ni was then deposited through physical vapor deposition onto the freshly cleaned surface. This was achieved by wrapping a Ni wire of 99.994% purity (Alfa Aesar) around a tungsten filament which was then resistively heated to a temperature above the vaporization point of Ni. The deposition of Ni was performed at 300 K, to kinetically trap the Ni atoms on the surface layer and create a surface similar to the starting surface in the MD simulations. The Auger Ni(849) to Pt(241 eV) peak ratio required to create 1 ML Ni was calculated using the method and inelastic mean free path values in Ref. 20, resulting in a value of 1.8. Ni was deposited until an Auger ratio of approximately 1.8 was achieved. After the surface was created at 300 K, the Ni/Pt(111) surface was flashed to 600 K, 700 K, 800 K, or 900 K at a heating rate of 6 K/s and then cooled to 500 K to take an Auger scan. The surface was then heated and held at the same temperature for approximately 20 min, with Auger scans taken from every 30 s to 5 min (the sample was cooled to 500 K for the Auger scans). Auger ratio values smaller than 1.8 would indicate that Ni

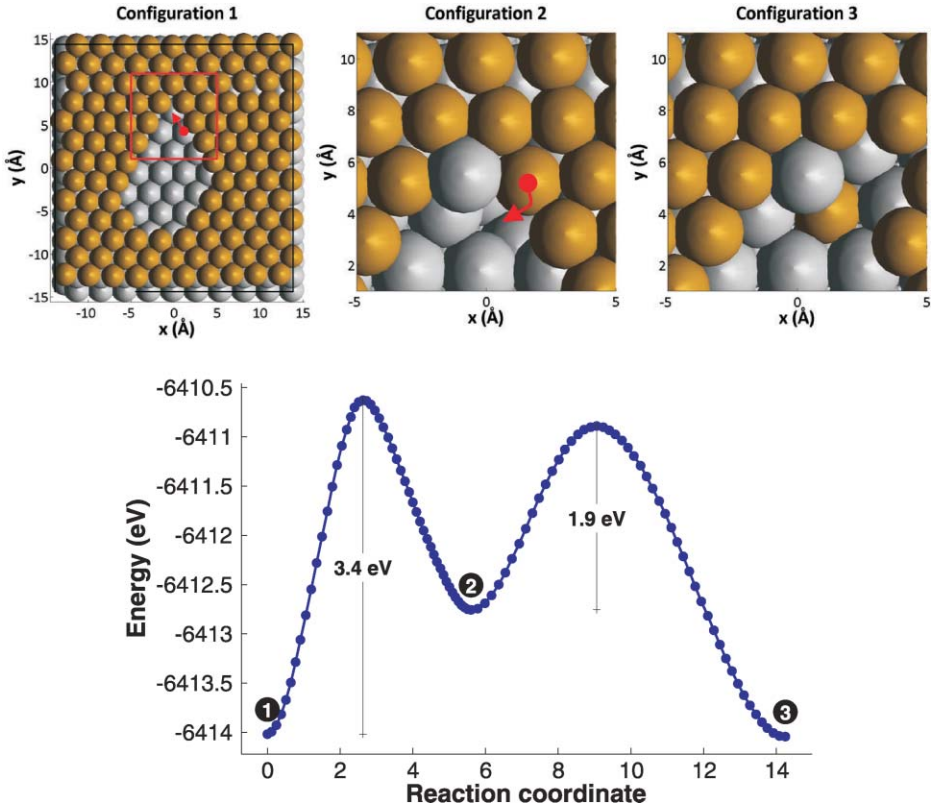

FIG. 1. The lattice mismatch between Ni and Pt results in the surface Ni atoms rearranging and creating defects or "holes" on the surface of the Pt catalyst as shown in configuration 1. A Pt atom migrates from the subsurface to the open holes on the top surface creating a vacancy in the first Pt layer (configuration 2). This process has an energy barrier of 3.4 eV. Subsequently, this vacancy can be filled by a Ni atom that hops from the surface to the first layer (configuration 3). The energy barrier of the latter process is 1.9 eV.

atoms on the top surface have diffused into the subsurface or bulk.

III. RESULTS AND DISCUSSION

A. NEB calculations

In order to estimate the energy barriers for Ni to diffuse from the top surface into the subsurface, we have carried out NEB calculations by considering three plausible mechanisms, each consisting of a number of elementary moves. We compute the potential energy profile along a minimum energy path connecting two, at the very least metastable, basins and passing through a saddle point in the potential energy surface. The path is parameterized by the arc length along it. The initial, or "reactant" state, is an energy-optimized configuration of the 1 ML Ni/Pt(111) system. The final, or "product" state, is one where a surface Ni atom has diffused from the surface to the second layer. Figure 1 shows the energy profile of one such path. Because of the lattice mismatch between Ni and Pt, optimization of the initial state results in the surface Ni atoms rearranging and creating defects or "holes" on the surface of the Pt catalyst (see configuration 1 in Fig. 1). The vacancies thus created on the Ni monolayer can "attract" Pt atoms from the first Pt layer. Because the Pt–Pt pairwise interaction in the EAM force field is stronger than the Ni–Pt one, by about 3 eV, the Pt atom has to overcome a substantial barrier of $E_a = 3.4$ eV to get to the surface. Such high diffusion barriers make it an improbable pathway for Ni diffusion at temperatures below 1000 K ($E_a \approx 36\,k_B T$ at $T = 1000$ K). This move creates a vacancy in the Pt layer (configuration 2) which can be filled by a Ni atom that hops down to the subsurface (configuration 3). The Ni atom has to surmount a 1.9 eV barrier to occupy that vacancy.

An alternative route for the Ni diffusion to the first Pt layer is shown in Fig. 2. In the first step, a Pt atom close to the left edge of the "hole" enters the surface layer. The energy barrier for this process, 1.7 eV, is much smaller than that for the transition between configurations 1 and 2 in Fig. 1 (3.4 eV). The reason is that in the current situation, the Pt atom is more exposed to the surface, and thus, has more space to move about and transition to the surface. Moreover, in the current case, the moving Pt atom has fewer immediate Ni neighbors, and thus, a lower energy cost is required to displace it. As a result of this transition, a vacancy is formed in the Pt layer. Subsequently, this vacancy diffuses to the right, when a Pt atom hops in the opposite direction overcoming a barrier of 1.1 eV (transition between configurations 1 and 2 in Fig. 2). Finally, a Ni atom from the surface monolayer fills this new vacancy; the energy barrier for this process is 1.9 eV. Note that the final state (configuration 3) looks like configuration 3 of Fig. 1.

The defects created in the surface layer of Ni undergo continuous rearrangements, and that process appears to facilitate Ni diffusion in the second layer, as shown in Fig. 3. Here we see that a Ni atom on the edge of the "hole" can hop to a

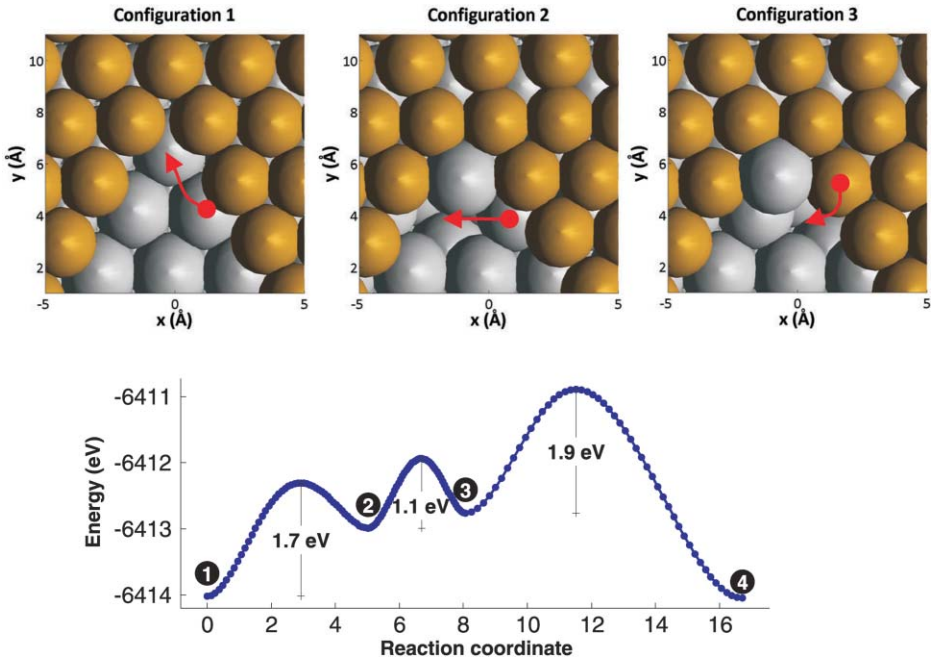

FIG. 2. Alternative route for the Ni diffusion to the 1st Pt layer: in the first step, a Pt atom close to the right edge of the "hole" enters the surface layer. Subsequently, a vacancy is formed in the first Pt layer, which diffuses to the right when a Pt atom hops in the opposite direction overcoming a barrier of 1.1 eV (transition between configurations 2 and 3). Finally, a Ni atom from the surface monolayer fills this vacancy. The final configuration looks like configuration 3 of Fig. 1.

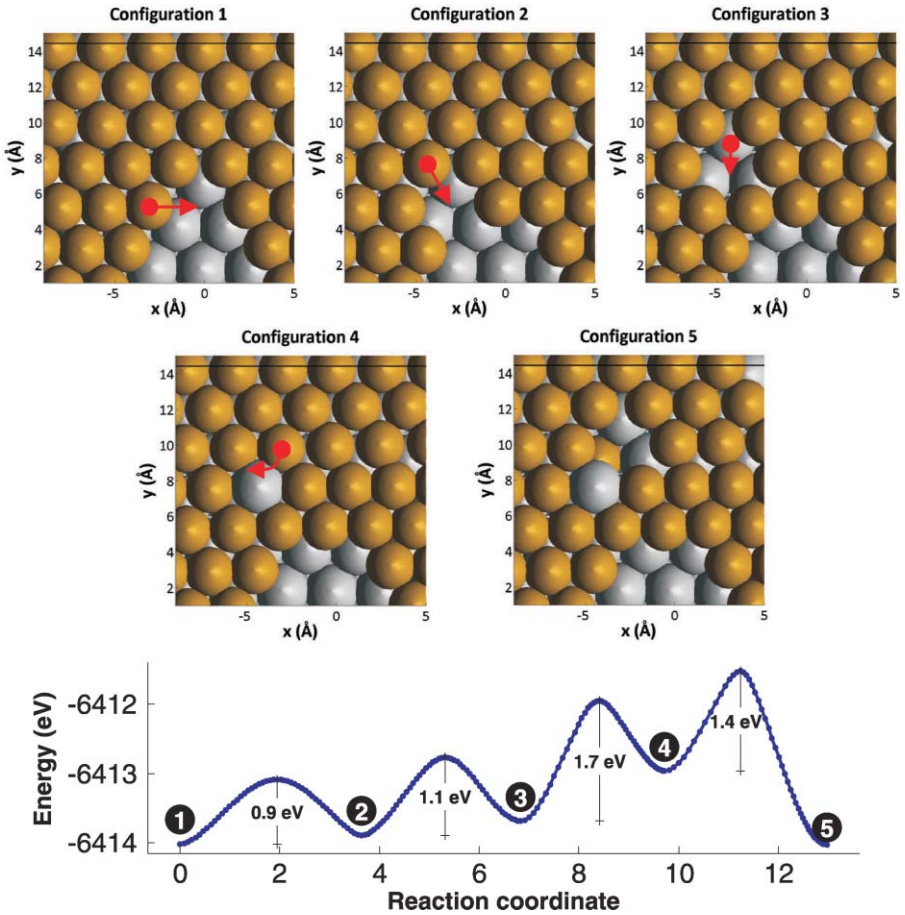

FIG. 3. The defects created in the surface layer of Ni undergo continuous rearrangements, which can facilitate Ni diffusion in the second layer. A Ni atom on the edge of the "hole" can hop to a neighboring position (configurations 1 and 2) by overcoming an energy barrier of 0.9 eV. A subsequent hop of another Ni atom can create a vacancy in the Ni rich area of the monolayer (configuration 3). The vacancy is now surrounded by six Ni atoms and can attract a Pt atom from the first layer to the surface with a barrier of 1.7 eV. A Ni atom subsequently hops to the created vacancy with an energy barrier of 1.4 eV.

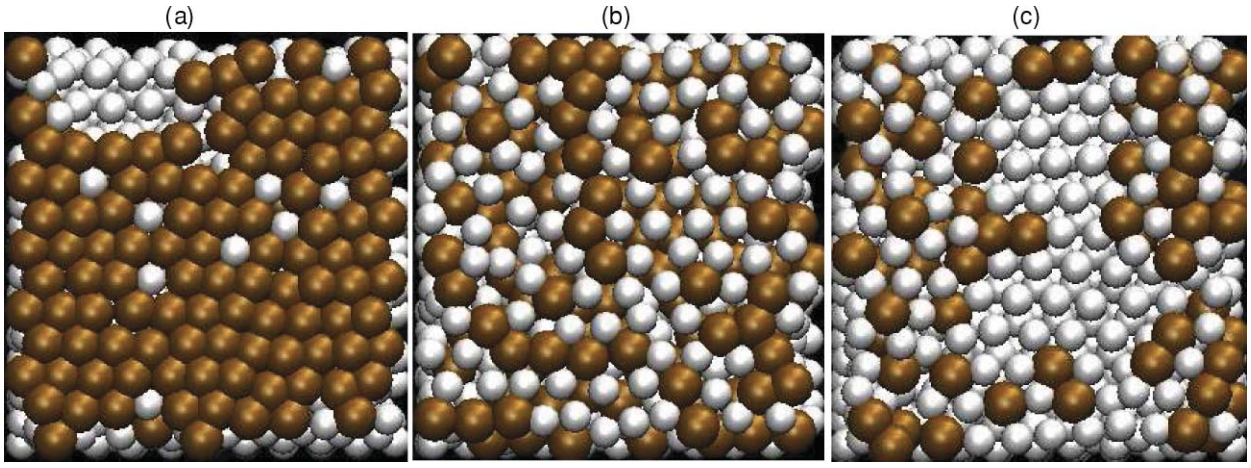

FIG. 4. Top views of the equilibrium Ni/Pt(111) structures after 30 ns MD simulation at constant temperature. (a) 1 ML at 900 K, (b) 1 ML at 1200 K, and (c) 1/2 ML at 900 K. Brown balls represent Ni atoms and white represent Pt atoms.

neighboring position (configurations 1 and 2) by overcoming a relatively low energy barrier of 0.9 eV. A subsequent hop of another Ni atom can create a vacancy in the Ni-rich area of the monolayer (configuration 3). The vacancy is now surrounded by six Ni atoms and can "attract" a Pt atom from the first Pt layer to the surface with a barrier of 1.7 eV. A neighboring surface Ni atom, with enough energy to overcome the 1.4 eV barrier, may subsequently hop into the newly created vacancy in the Pt layer. This mechanism, which involves correlated hops of Ni atoms, has a maximum barrier of 1.7 eV, thereby constitutes a more probable path compared to the previous two. Based on this barrier and employing classical transition state theory (TST), we estimate the time scale of Ni diffusion to be around 3 min at 600 K and around 2 μs at 900 K. These values compare well with the experimental data shown later, which show timescales of the order of minutes at 600 K and shorter than a second at 900 K.

While the pathways studied are not exhaustive of what may happen in an actual system, the three mechanisms presented above suggest that the elementary steps associated with the mixing process between Ni and Pt involve: the formation of defects of "holes" in the Ni monolayer; the subsequent displacement of Pt atoms from the subsurface and the formation of vacancies therein; and finally the migration of Ni atoms to fill them. Direct diffusion mechanisms entail quite high activation barriers, whereas vacancy creation carries a relatively smaller energetic cost when it involves the correlated motion of a number of Ni atoms. Later, we will demonstrate by means of the van Hove correlation function on MD trajectories that Ni diffusion does indeed take place via a correlated hopping mechanism.

B. MOLECULAR DYNAMICS (MD) SIMULATIONS

1. Ni layer stability versus temperature

In this section, we focus on characterizing the metastable and stable states after Ni and Pt have been mixed at various temperatures. We have used MD to investigate the behavior of the Ni layer at various temperatures. Specifically, and on account of the activation barriers that we obtained from the NEB calculations, we have considered temperatures within the range of 900–1300 K. At lower temperatures, e.g., 600 K, and a full Ni monolayer, the MD trajectories have shown no Ni diffusion into the subsurface. That was anticipated, as the system gets trapped in long-lived, metastable basins of the potential energy surface and low-temperature escape from such states of metastability cannot be captured by ns-long MD trajectories.

At elevated temperatures, 30-ns long trajectories show that the Ni atoms diffuse to the subsurface, but we do not observe any diffusion into the bulk of the catalyst. At $T = 900$ K [Fig. 4(a)], a few Ni atoms (less than 7%) diffuse to the subsurface layer, while those that remain on the surface reorganize to conform to the Ni lattice constant, creating a hole that exposes the Pt of the subsurface layer. At the higher temperature of $T=1200$ K [Fig. 4(b)], the population of Ni atoms in the subsurface layer increases, as a lot of them have enough thermal energy to overcome the diffusion barrier—but apparently not enough to further migrate into the bulk.

Figure 5 shows the coordination numbers (CN) for the atom pairs Pt–Pt, Pt–Ni, Ni–Pt and Ni–Ni at four different temperatures. At $T = 900$ K, the coordination numbers for Ni–Pt and Ni–Ni, out to a radius of 3 Å, are about 3 and 5, respectively. The former is a result of the fact that most of the Ni stays at the surface and, on average, has three Pt nearest neighbors, all in the second layer. For the Ni–Ni pair, a Ni atom should be coordinated with six Ni atoms in a perfect layer. The actual average coordination number of 5, that we compute here is the result of the holes that form on the surface as the Ni atoms reorganize to conform to their own lattice, whose constant is about 10% smaller than that of Pt. As the temperature increases, and as we can see from Figs. 5(b)–5(d), the Pt coordination around Ni (labeled as Ni–Pt) increases, while that of Ni around Ni (labeled as Ni–Ni) decreases. This is because Ni atoms, originally on the surface layer, diffuse into the subsurface.

The temperature effects on the structure of the bimetallic can be more clearly seen from the time evolution of the

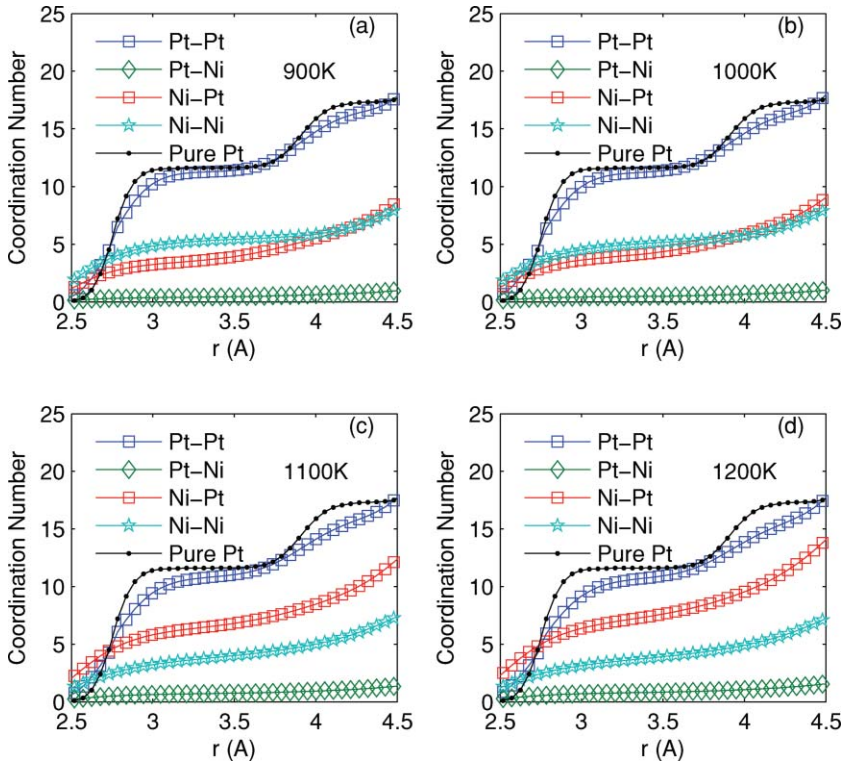

FIG. 5. Coordination numbers (CN) of Pt–Pt, Pt–Ni, Ni–Pt, and Ni–Ni in the 1 ML Ni/Pt(111) system at 900 K (a), 1000 K (b), 1100 K (c), 1200 K (d). The coordination number for Pt–Pt in pure Pt bulk is also shown for comparison purposes.

Ni–Ni and Ni–Pt coordination numbers along the entire MD trajectory, namely, including the equilibration period. These time series are shown in Figures 6(a) and 6(b), for $T = 900$ K and $T = 1200$ K, respectively. In essence, we follow the relaxation of the system from a state that corresponds to the preparation of the bimetallic in the laboratory. At 900 K, we observe practically no changes for the duration of the trajectory. However, at 1200 K, the Ni–Ni coordination quickly drops to around 3.5, after about 10 ns, while the Ni–Pt coordination increases to over six, after about 15 ns. The coordination numbers then reach a plateau, indicating a metastable state has been reached, as we will discuss later. Based on the estimated time scales from the NEB calculations, it is clear that at higher temperatures (e.g., 1200 K), thermal fluctuations "open up" the structure and create lower diffusion barriers that allow some mixing of Ni and Pt at ns time scale.

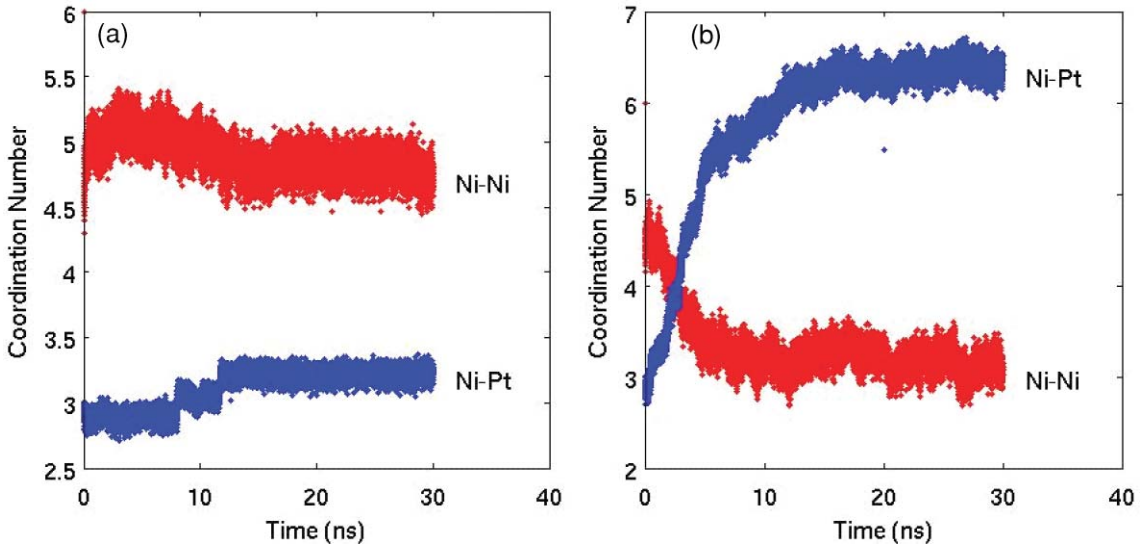

FIG. 6. Time evolution of Ni–Ni and Ni–Pt coordination number at 3 Å. (a) 900 K and (b) 1200 K. 3 Å is the distance chosen to include all the first nearest neighbors when counting CN.

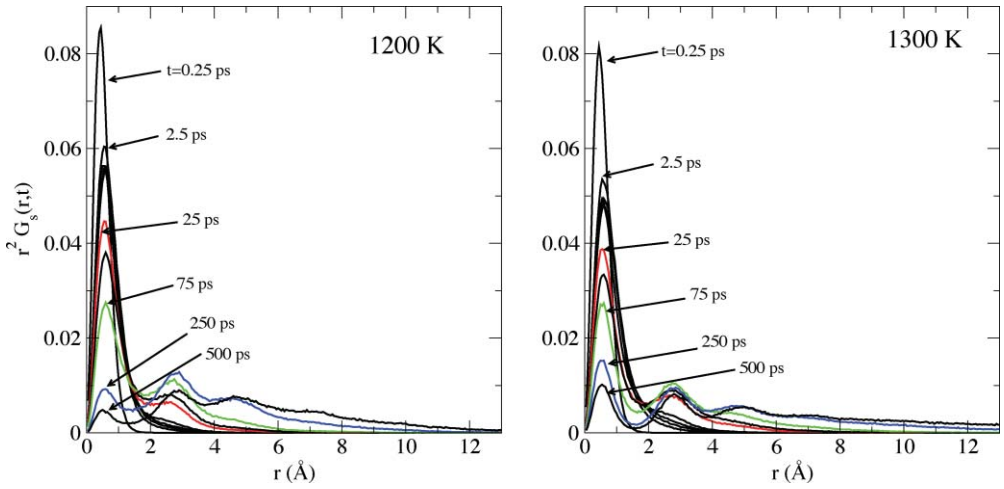

FIG. 7. Self part of the van Hove correlation function ($G_s(\vec{r}, t)$) for the Ni atoms as a function of r graphed at different times t, for $T = 1200$ and 1300 K. Some curves are in color for visual aid.

2. Ni diffusion mechanism

Analysis of the NEB calculations suggested that Ni diffusion via correlated hops entails a lower energetic cost. To further investigate the relaxation of the Ni atoms, it is of interest to examine the temporal evolution of the probability to find a Ni atom some distance, say r, away from a space point it occupied at an earlier time. This is formally given by the self (or incoherent) part of the van Hove correlation function.[21] For classical systems, the van Hove correlation function is given by the ensemble average

$$G(\vec{r}, t) = \left\langle \frac{1}{N} \sum_{i=1}^{N} \sum_{j=1}^{N} \delta(\vec{r} + \vec{r}_i(0) - \vec{r}_j(t)) \right\rangle , \tag{3}$$

where N is the number of particles, $\vec{r}$ denotes position vector and $\delta(x)$ is the Dirac δ-function. The self part of the correlator, $G_s(\vec{r}, t)$, which we analyze for the Ni atoms, is given by the diagonal terms ($i = j$) in the summation. It is worth mentioning that the second moment of the probability density $G_s(\vec{r}, t)$ gives us the mean square displacement, $\langle|\vec{r}(t) - \vec{r}(0)|^2\rangle$, of the Ni atoms.

In Fig. 7 we graph the probability $G_s(r, t)r^2\mathrm{d}r$ for the Ni atoms at 1200 and 1300 K. For simple diffusive motion, the probability $G_s(r, t)r^2\mathrm{d}r$ should be a unimodal, bell-shaped curve which, with time, should become flatter. In fact, at very short times (the so-called ballistic regime), its center should shift to larger r like $\propto t$, while at times longer than the characteristic time scale for microscopic relaxation the center should move to the right like $\propto \sqrt{t}$. For both temperatures considered in the figure, we see that at short times ($t < 5$ ps) the probability is unimodal with a slowly shifting center. In fact, at the lower temperature of 1200 K, we observe that the shift is somewhat slower than at 1300 K. Thus, at such short times, the Ni atoms oscillate about their equilibrium positions and not much else is happening. Soon, however, the probability begins to develop a second peak, roughly 2.2 Å away from the main one; at $t \approx 75$ ps, it is clearly bimodal. The main peak, at short r, decreases in amplitude—as it should because of particle conservation—but, interestingly, it does *not* shift outward. This structure of the $G_s(\vec{r}, t)$ signifies that Ni diffuses via a mechanism of correlated hops. The very weak time dependence of the location of the peak at short r reveals a "cage effect", i.e., the particles are trapped by their neighbors and oscillate about their positions. With time, however, a trapped Ni atom does not quite escape from the "cage" but rather it hops to the position of one of its nearest neighbors in a highly correlated fashion. At longer times, we see that $G_s(\vec{r}, t)$ develops more structure, namely, new peaks appear at large r, albeit broader and less intense. We should note that this diffusive motion by correlated hops persists at lower Ni coverages.

3. Equilibrium structures from simulated annealing

Clearly, the Ni layer is not stable and diffusion into the subsurface occurs on the nanosecond time scale. The system, however, appears trapped in that state with no further Ni migration into the bulk taking place. The NEB calculations and the analysis of the van Hove correlation function have revealed that Ni diffusion happens by correlated hops involving its neighbors and requiring the formation of vacancies. Thus, one should expect higher barriers for diffusion in the bulk, and time scales not accessible by constant temperature MD trajectories.

In Fig. 8, we show the structure obtained from simulated annealing simulations. (Similar structures, not shown here,

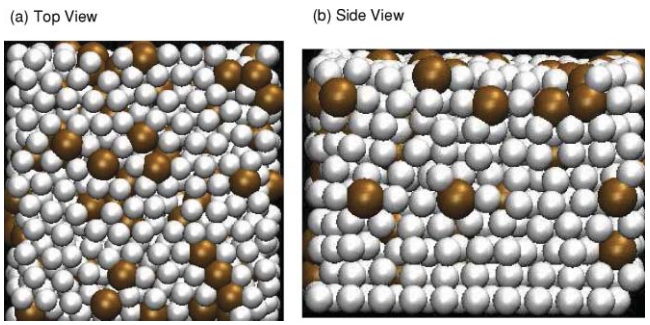

FIG. 8. Top and side views of the equilibrium structure of 1 ML Ni/Pt(111) at 900 K obtained by simulated annealing.

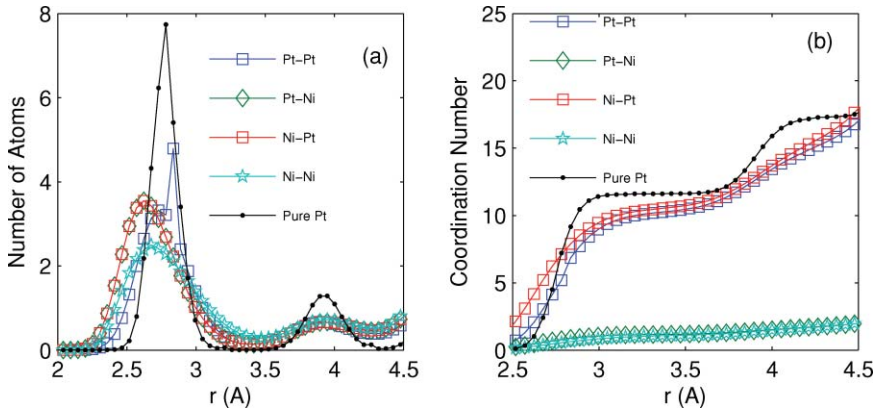

FIG. 9. (a) Radial distribution function (RDF) and (b) coordination number (CN) for the equilibrated 1 ML Ni/Pt(111) at 900 K obtained by simulated annealing. RDF and CN of pure Pt bulk at 300 K are also plotted for comparison.

are obtained at lower temperatures too.) About 10% of the Ni atoms remain on the surface, as seen in the top-view panel in Fig. 8(a). The rest diffuse into the bulk of Pt and associate mostly with Pt atoms, as suggested by the side-view panel in Fig. 8(b). Although some Ni dimers and trimers exist, it seems that the Ni atoms tend to avoid each other, leading to a fairly uniform distribution, probably to maximize the configurational entropy.

Figure 9(a) shows the radial distribution functions (RDF) for the atom pairs Pt–Pt, Pt–Ni, Ni–Pt, and Ni–Ni in the 1 ML Ni/Pt(111) system; the Pt–Pt RDF of a pure Pt slab at 300 K has also been included for comparison. Characteristic fcc peaks are present in all the RDFs that we show here. In particular, we notice that the Ni–Ni, Ni–Pt, and Pt–Ni RDF have peaks at the same locations, indicating that Ni and Pt form a disordered, fcc-solid solution. This is consistent with the Ni–Pt phase diagram,[22,23] at $T = 900$ K and the Ni/Pt ratio considered here, namely, 88.9% Pt (excluding the bottom Pt layer, which was kept frozen during the simulations). Simulations with different Ni initial configurations led to a similar disordered, fcc-solid solution. We also see that the main peak of the Pt–Pt RDF, located at 2.80 Å, has a shoulder at 2.70 Å. The peak at 2.80 Å is also present in the Pt–Pt RDF for a pure Pt slab, corresponding to the Pt lattice constant of 3.92 Å. The shoulder at 2.70 Å is due to the Ni–Pt lattice mismatch and reveals that some Pt atoms readjust their positions in order to conform to the Ni lattice constant. This is also evidenced by the fact that the main peak in the Ni–Ni RDF is located at ~2.70 Å. The corresponding coordination numbers are shown in Fig. 9(b). From the Ni–Ni RDF, we find that, on average, each Ni atom has only ~0.5 Ni nearest neighbors, clearly showing that Ni is well dispersed in Pt. This is further confirmed by the fact that, beyond the 3 Å radius, the coordination numbers for the atom pairs Pt–Pt, Pt–Ni, and Ni–Pt are practically the same.

In Fig. 10 we plot the percentage of Ni in each layer. Interestingly, the Ni concentration oscillates from one layer to the other. Although the majority of the Ni atoms diffuse into the Pt bulk, a small amount (≈10%) of Ni remains at the surface. This is consistent with conclusions drawn from the analysis of STM images, LEIS and AES ratio measurements for 1 ML Ni on Pt(111).[11] Furthermore, we see that the Ni concentration in the second layer (subsurface) is as high as 21%, almost double of that in the first layer. Similar Ni enrichment of the subsurface has been observed using Monte Carlo simulations of $Pt_{50}Ni_{50}$.[24] Pt enrichment of the top surface and Ni enrichment of the subsurface have also been experimentally observed for the $Pt_3Ni(111)$ catalyst.[25,26] A possible explanation for this behavior is that Pt has a lower surface energy than Ni.[27,28]

4. Coverage effects

As we have already pointed out, at 1 ML Ni coverage and $T = 900$ K, only a small fraction of Ni atoms diffuse to the subsurface in 30 ns [see Fig. 4(a)]. In contrast, at the same temperature, more facile Ni diffusion to the subsurface occurs when the coverage of Ni is reduced to 1/2 ML, as shown in Figure 4(c). This is because, in the 1/2 ML case, there is more open space for the exchange between a Pt atom in the subsurface and a Ni atom at the top surface. For a Ni atom to take

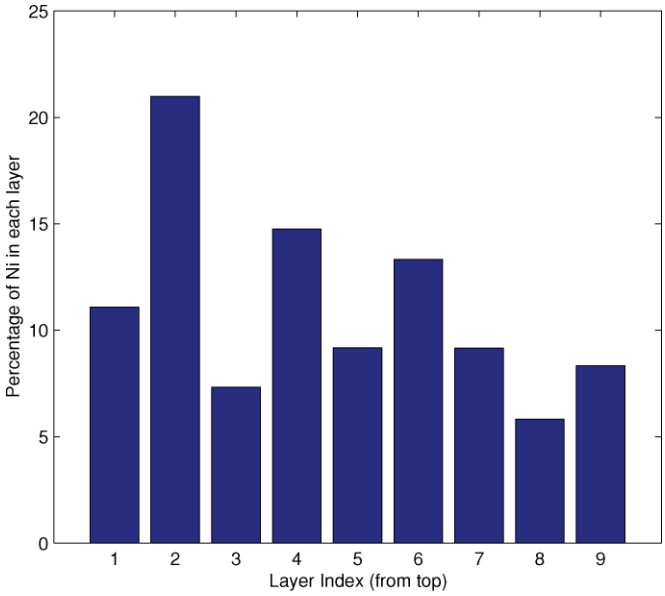

FIG. 10. Percentage of Ni in each layer after the Ni/Pt(111) is equilibrated through simulated annealing. The layer number is indexed from top surface and the bottom layer is not shown since it is frozen.

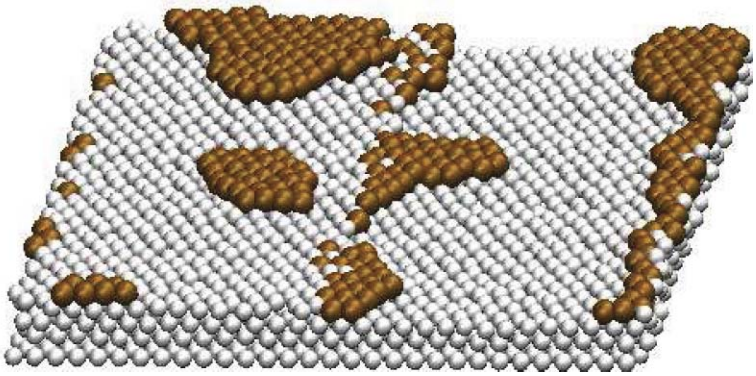

FIG. 11. MD simulated equilibrium structure for 0.25 ML Ni on stepped Pt(111) at 600 K. Mixing between Ni and Pt is observed along the Pt step edge.

the place of a Pt atom in the subsurface layer, a vacancy must first form. In the absence of full Ni monolayer, a Pt atom can easily move up a level, thus creating the necessary vacancy to be occupied by the migrating Ni atom. In other words, the effective barrier for this to occur is lower at 1/2 ML than at 1 ML.

For coverages higher than 1 ML, Ni and Pt do not mix at all at 900 K. At 1 ML, we have seen that the Ni–Pt lattice mismatch leads to the formation of surface vacancies which expose the subsurface Pt [see Fig. 4(a)]. At 2 ML Ni coverage, these vacancies are filled with Ni atoms from the second (upper) Ni layer (picture not shown). This effectively closes the available diffusion channels. At higher temperatures, mixing between Ni and Pt takes place at 2 or even 3 ML coverages.

5. Step effects

At submonolayer coverage, some mixing between the Ni and Pt atoms in the Ni/Pt(111) takes place at 900 K, but at 600 K no mixing was observed for 1/2 ML Ni/Pt(111) during a 30-ns MD simulation. Kitchin *et al.* have observed that Ni atoms deposited at 300 K remain on the Pt(111) surface but diffuse into the Pt bulk at 600 K.[11] On the other hand, Gambardella and Kern have observed that Ni can still exchange with Pt, even at temperatures lower than 300 K, when Ni is deposited to *vicinal* Pt(111).[29] This suggests that the presence of steps can facilitate mixing. In order to test this hypothesis, we created a Pt step, by removing half of the top Pt layer, and then randomly deposited 0.25 ML of Ni atoms on the stepped Pt(111) surface. In order to minimize periodic-boundary effects, and thus, the interaction between steps, we increased the simulation box size to 8.32 nm × 8.64 nm. As shown in Fig. 11, Ni atoms on a terrace do not mix with Pt, but instead prefer to form nanoparticles. However, Ni atoms along the edges of the Pt steps start mixing with Pt. This is probably because the Pt atoms along the step edge are undercoordinated, and thus, not so strongly bound. Hence, it is easier for them to diffuse away to give way to Ni atoms. This finding is in agreement with the mechanism proposed by Gambardella and Kern[29] to describe the kinetically-limited exchange between Ni and Pt along step edges.

C. Comparison between experiments and simulations

In order to compare the overall trends found in simulations, we performed a series of experiments at various temperatures after preparing the 1 ML Ni/Pt(111) system to characterize the amount of Ni left on the surface using AES. Approximately, 1 ML Ni corresponds to an Auger ratio of around 1.8 as calculated by the method of Cumpson and Seah.[20,30]

As shown in Fig. 12, after flashing the Ni/Pt(111) surface to 600 K, the Auger ratio decreased to approximately 1.3 and further decreased to 1.2 after 10 min. If a structure is assumed, a theoretical Auger ratio can be calculated. For a Ni metal layer in the subsurface configuration (a layer of Pt, with a layer of Ni underneath it and a Pt bulk), the theoretical Auger ratio can be calculated as[31]

$$\frac{I_{\mathrm{Ni}}}{I_{\mathrm{Pt}}} = \frac{S_{\mathrm{Ni}}[1 - f(\mathrm{Ni}, \mathrm{Ni})]f(\mathrm{Pt}, \mathrm{Ni})}{S_{\mathrm{Pt}}[f(\mathrm{Ni}, \mathrm{Pt})f(\mathrm{Pt}, \mathrm{Pt}) + 1 - f(\mathrm{Pt}, \mathrm{Pt})]}, \tag{4}$$

where $f(\mathrm{M}_1, \mathrm{M}_2) = \exp[-d_{\mathrm{M}_1}/\lambda_{\mathrm{M}_1}(E_{\mathrm{M}_2})\cos\theta]$, S is the sensitivity, d is the effective thickness, $\lambda(E_{\mathrm{M}})$ is the mean free path of the Auger electron with energy E through metal M, and $\cos\theta$ is a term introduced to account for the solid acceptance angle of the cylindrical mirror analyzer (CMA), which is 42.3° for the single-pass CMA used in this work. The calculated Auger ratio for Ni subsurface configuration is 1.4. At

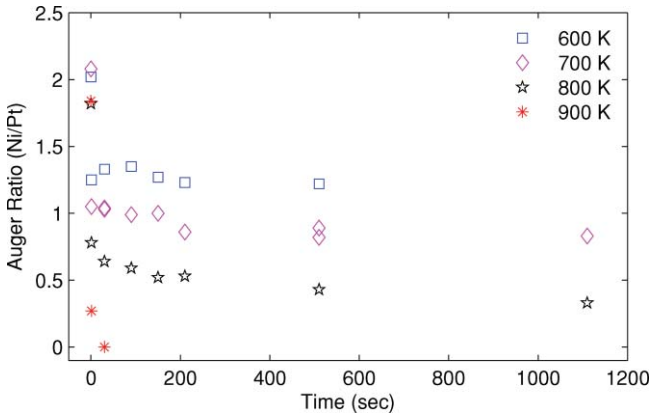

FIG. 12. Time evolution of the Auger ratio (Ni/Pt) for 1 ML Ni/Pt(111) bimetallic catalyst at various temperatures. Approximately 1 ML Ni corresponds to an Auger ratio of around 1.8, and smaller values in Auger ratio indicate diffusion of Ni atoms to the subsurface or even the Pt bulk.

600 K, a layer of Ni in the second layer is consistent with the experimental results, although is not conclusive, since the Auger technique is sensitive up to approximately 30 Å, with higher sensitivity in the top most layers. Although the temperatures in experiments are around 300 K lower than those in MD simulations to observe the onset of mixing, the results are consistent with the MD findings of a system with a metastable state where the Ni atoms reside in the second layer, sandwiched by a Pt rich surface layer and the Pt bulk [see Fig. 4(b)].

After initially flashing the surface to 700 K, the Auger ratio decreases to 1.0 and further decreases to 0.8 after 20 min. This is below the value for 1 ML of Ni in the second layer and appears that some Ni stays in the second layer, while some also diffuses into the bulk. The initial drop after flashing the temperature to 800 K is from 1.8 to 0.8 and the Auger ratio continues to decrease to 0.3 over the 20 min interval. It is clear that Ni atoms are no longer trapped in the metastable second layer, but are now diffusing into the bulk. At 900 K, the Ni signal is below the detection limit of AES within 30 seconds, indicating Ni rapidly diffuses into the bulk. From the simulated annealing calculations, there is an even distribution of Ni in all layers, except the second layer is Ni rich. This is not seen in the 900 K case because there is an infinite number of bulk layers, and the Ni fraction in each layer approaches zero when heated. At 600–800 K, some mixing happens at time scales shorter than a second that cannot be resolved experimentally. This first transient regime is followed by mixing over a slower (minute) time scale. At higher temperatures (e.g., 900 K), mixing is complete at very short (unresolved) time scales.

The above comparison demonstrates that temperature indeed plays a critical role in determining how Ni and Pt mix: the Ni atoms remain at the top surface at low temperatures, while at intermediate temperatures they diffuse into the subsurface layer and remain trapped for a long period of time; diffusion all the way into the bulk to reach low-lying energy basins occurs only at high temperatures. Exact match in temperatures between these experiments, on the scale of minutes, and the MD simulations, on the scale of nanosecond, is currently very challenging. Nevertheless, the relative trends of the temperature effects from experiment and simulation agree well.

IV. CONCLUSIONS

We have studied the mixing of Ni and Pt in the Ni/Pt(111) bimetallic surfaces by molecular simulation employing embedded atom method potentials. We used a variety of computational tools as well as UHV experiments to probe different time scales. We have seen that Ni diffusion from the top surface to the subsurface layer is kinetically unlikely unless open structures form and more concerted mechanisms are explored. This was suggested by analysis of the energy landsacape via NEB calculations and verified by analyzing the Ni relaxation dynamics by computing the van Hove correlation function, which revealed that Ni diffusion happens via a correlated hopping mechanism. MD simulations up to 30 ns showed that higher temperatures, smaller Ni coverages and Pt steps facilitate mixing between Ni and Pt. At low temperatures, all Ni atoms remain trapped on the top surface due to large diffusion barriers and possibly significant energy dissipation through the long-wavelength Pt acoustic phonons. At intermediate temperatures, the majority of Ni atoms diffuse into the second layer, forming a subsurface configuration. At high enough temperatures, Ni atoms diffuse into the Pt bulk and reach equilibrium, consistent with the simulated annealing calculations.

Overall, mixing entails multiple time scales: at short times, mixing from the top layer to the second layer occurs by overcoming fairly large barriers via correlated hopping mechanisms. This leads to metastable structures with Ni being present in both layers. Further mixing in deeper layers involves even higher barriers and requires much longer time scales than those accessible via MD simulations at typical temperatures. Under these conditions, Ni is present in all layers with a Ni-enrichment in the second layer.

ACKNOWLEDGMENTS

The MD work was conducted by H.W. and was supported from National Science Foundation (NSF), grant (CMMI-0835673). The NEB work was conducted by M.S. and the experimental work by D.A.H. supported by the Department of Energy (DOE) under grants (DE-FG02-05ER25702 and DE-FG02-06ER15795), respectively. The time correlation and supervision of part of the MD and NEB work was conducted by S.C. based upon work financially supported as part of the Catalysis Center for Energy Innovation, an Energy Frontier Research Center funded by the U.S. Department of Energy, Office of Science, Office of Basic Energy Sciences under Award No. DE-SC0001004.

[1] Y.-H. Chin, D. King, H.-S. Roh, Y. Wang, and S. M. Heald, J. Catal. **244**, 153 (2006).
[2] V. R. Stamenkovic, B. S. Mun, K. J. J. Mayrhofer, P. N. Ross, and N. M. Markovic, J. Am. Chem. Soc. **128**, 8813 (2006).
[3] J. Zhang, K. Sasaki, E. Sutter, and R. R. Adzic, Science **315**, 220 (2007).
[4] J. G. Chen, C. A. Menning, and M. B. Zellner, Surf. Sci. Rep. **63**, 201 (2008).
[5] J. A. Rodriguez and D. W. Goodman, Science **257**, 897 (1992).
[6] B. Frühberger, J. E. Jr, and J. G. Chen, Catal. Lett. **45**, 85 (1997).
[7] S. Lu, W. W. Lonergan, J. P. Bosco, S. Wang, Y. Zhu, Y. Xie, and J. G. Chen, J. Catal. **259**, 260 (2008).
[8] Y. Shu, L. E. Murillo, J. P. Bosco, W. Huang, A. I. Frenkel, and J. G. Chen, Appl. Catal. A: General **339**, 169 (2008).
[9] D. A. Hansgen, D. G. Vlachos, and J. G. Chen, Nat. Chem. **2**, 484 (2010).
[10] O. Skoplyak, C. A. Menning, M. A. Barteau, and J. G. Chen, Top. Catal. **51**, 49 (2008).
[11] J. R. Kitchin, N. A. Khan, M. A. Barteau, J. G. Chen, B. Yakshinskiy, and T. E. Madey, Surf. Sci. **544**, 295 (2003).
[12] C. A. Menning and J. G. Chen, J. Chem. Phys. **128**, 164703 (2008).
[13] http://lammps.sandia.gov/.
[14] S. M. Foilses, M. I. Baskes, and M. S. Daw, Phys. Rev. B **33**, 7983 (1986).
[15] M. S. Daw and M. I. Baskes, Phys. Rev. Lett. **50**, 1285 (1983).
[16] M. S. Daw and M. I. Baskes, Phys. Rev. B **29**, 6443 (1984).
[17] L. Verlet, Phys. Rev. **159**, 98 (1967).
[18] G. Henkelman and H. Jonsson, J. Chem. Phys. **113**, 9978 (2000).
[19] W. Smith, T. R. Forester, and I. T. Todorov (website: http://www.cse.scitech.ac.uk/ccg/software/DL_POLY/).
[20] P. J. Cumpson and M. P. Seah, Surf. Interface Anal. **25**, 430 (1997).
[21] L. van Hove, Phys. Rev. **95**, 249 (1954).
[22] C. E. Dahmani, M. C. Cadeville, J. M. Sanchez, and J. L. Morán-López, Phys. Rev. Lett. **55**, 1208 (1985).

[23]W. Gong, L. Zhang, D. Yao, and C. Zhou, Scr. Mater. **61**, 100 (2009).
[24]G. Wang, M. A. V. Hove, P. N. Ross, and M. I. Baskes, J. Chem. Phys. **122**, 024706 (2005).
[25]V. Stamenkovic, T. J. Schmidt, P. N. Ross, and N. M. Markovic, J. Phys. Chem. B **106**, 11970 (2002).
[26]V. R. Stamenkovic, B. Fowler, B. S. Mun, G. Wang, P. N. Ross, C. A. Lucas, and N. M. Markovic, Science **315**, 1135941 (2007).
[27]W. R. Tyson and W. A. Miller, Surf. Sci. **62**, 267 (1977).
[28]F. R. de Boer, R. Room, W. C. Mattens, A. R. Miedema, and A. K. Niessen, *Cohension in Metals* (North-Holland, Amsterdam, 1988).
[29]P. Gambardella and K. Kern, Surf. Sci. **475**, L229 (2001).
[30]C. J. Powell and A. Jablonski, Surf. Interface Anal. **29**, 108 (2000).
[31]M. P. Humbert, "Catalytic properties of platinum and tungsten carbide-based bimetallic surfaces," Ph.D. thesis, University of Delaware: Newark, 2009.